ChemCatChem

Review
doi.org/10.1002/cctc.202400125

Chemistry Europe
European Chemical Societies Publishing

www.chemcatchem.org

Interface Engineering of Electrocatalysts for Efficient and Selective Oxygen Evolution in Alkaline/Seawater

Daekyu Kim,[a] Wenhan Zu,[a] Ching Lam Kwok,[a] and Lawrence Yoon Suk Lee*[a, b]

Electrochemical water splitting is regarded as an effective technology for producing green hydrogen, which is crucial for addressing energy and environmental challenges. In particular, direct seawater splitting offers significant economic and environmental advantages. However, its efficiency is hindered by the high overpotential required for the oxygen evolution reaction (OER) and the competition from chloride oxidation. This review highlights the potential of interface engineering to overcome these limitations and develop efficient OER electrocatalysts. We comprehensively explore recent advancements in interface engineering for OER in both alkaline and seawater environments. We begin by introducing the mechanisms of freshwater and seawater electrolysis, emphasizing key considerations for OER catalyst design. Subsequently, we review the recent progress made in various interface engineering strategies, analyzing their impact on OER performance in both electrolytes. Finally, we outline promising future directions for developing efficient seawater oxidation catalysts through interface engineering.

1. Introduction

The extensive utilization of fossil fuels to fulfill global energy demand has resulted in energy crises and environmental degradation.[1,2] The development of clean and sustainable energy sources is of utmost importance for our generation. In this context, hydrogen has emerged as a promising future energy source due to its high energy density of 142 MJ kg^{-1} and environmentally benign nature.[3,4] Currently, global hydrogen production heavily relies on fossil fuel reforming, leading to the emission of CO_2.[5] Electrolytic water splitting has attracted huge attention as it offers the advantage of producing high-purity hydrogen without CO_2 emissions.[6,7] However, the sluggish kinetics of the anodic oxygen evolution reaction (OER) and the reliance on precious metals such as RuO_2 and IrO_2 are the main obstacles that hinder the widespread application of water electrolysis.[8–10] Another challenge in water electrolysis is the requirement of high-purity freshwater, which is becoming increasingly difficult to secure due to global population growth and severe water pollution.[11,12]

Seawater, which constitutes approximately 97% of the Earth's total water, is considered an ideal resource for hydrogen production through electrolysis.[13] Moreover, seawater contains various ionic substances, including Cl^-, Na^+, SO_4^{2-}, Mg^{2+}, Ca^{2+}, and K^+ ions, with a concentration of *ca.* 3.5 wt.%, making it more conductive than freshwater.[14,15] However, the existence of impurities such as micro-precipitate, organic molecules, and microorganisms can have unpredictable adverse effects.[14,16] A more significant challenge comes from the chloride content in seawater, which is close to 0.5 M. Chlorides can be easily oxidized to form various chlorine species depending on the pH (Figure 1),[17] and these reactions are known as chlorine oxidation reactions (COR). COR competes with the OER, resulting in severe electrode corrosion and reduced OER efficiency. To mitigate COR during seawater electrolysis, it is necessary to increase the OER selectivity by widening the potential gap between OER and COR.[17] According to the Pourbaix diagram for artificial seawater (Figure 1), the potential

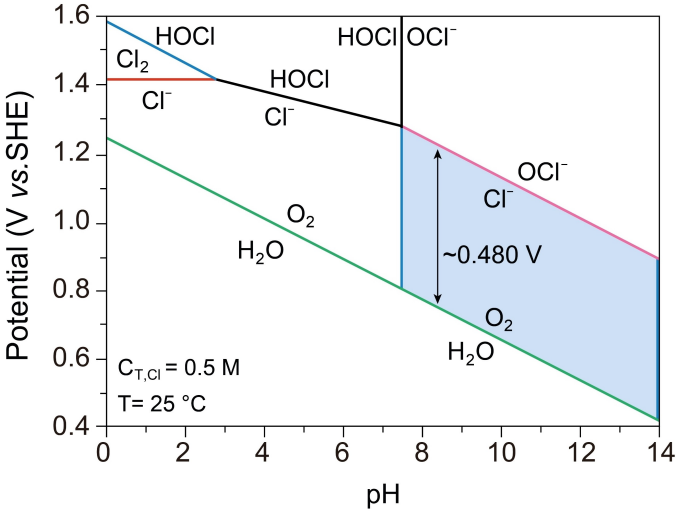

Figure 1. Pourbaix diagram of seawater oxidation model in simulated seawater with 0.5 M NaCl. Reproduced with permission.[17] Copyright 2016, Wiley-VCH.

[a] *D. Kim, W. Zu, C. Lam Kwok, L. Y. S. Lee*
Department of Applied Biology and Chemical Technology and Research Institute for Smart Energy, The Hong Kong Polytechnic University, Hung Hom, Kowloon, Hong Kong SAR
E-mail: lawrence.ys.lee@polyu.edu.hk

[b] *L. Y. S. Lee*
Hong Kong Polytechnic University Shenzhen Research Institute, Nanshan, Shenzhen, Guangdong, China, 518057

gap is extended and reaches approximately 480 mV in alkaline media ($7.5 < pH < 14$). Maintaining an alkaline environment is recommended to suppress COR in seawater. However, considering that COR exhibits superior reaction kinetics compared to OER, it becomes challenging to completely prevent COR during long-term operation at high current densities in practical applications.[18,19] Therefore, it is crucial to develop OER catalysts that are resistant to chlorine, exhibit high selectivity, and demonstrate stability under high current densities to enable the widespread use of seawater electrolysis.

Interface engineering has emerged as an effective strategy for improving the performance of electrocatalysts, as electrochemical reactions occur at the interface between the catalyst surface and electrolyte.[20–22] The interface, which is formed by hybridizing two or more distinct components can provide mass transfer channels and adsorption sites for reaction intermediates.[20,23] Tuning the atomic configurations at the interfaces allows for modulation of the physicochemical properties of electrocatalysts, leading to enhanced activity and stability.[24–30] The intimate coupling of different components at the interface can modify electronic structures, improving charge transfer, optimizing binding interactions with intermediates, and enhancing catalytic stability.[24,31,32] Consequently, significant research efforts have focused on designing electrocatalysts through interface engineering.[32,33] However, few studies have comprehensively covered the various interface configurations and their specific impact on OER activity in an alkaline seawater environment. Therefore, there is a timely and necessary need for a review addressing this knowledge gap.

This review aims to comprehensively explore the design strategies of electrocatalysts for alkaline seawater oxidation through interface engineering. We begin by providing a brief introduction to the fundamentals of water electrolysis. Subsequently, we discuss the theoretical aspects of seawater electrolysis and highlight the challenges associated with seawater oxidation, which helps establish the design requirements for electrocatalysts. We then elaborate on the classification of interface configurations and the effects of interfaces and showcase the achievements made in developing electrocatalysts for the OER in both alkaline and seawater conditions. Finally, we conclude the review by offering perspectives on the challenges and future directions of interface engineering research for electrocatalysts in direct seawater electrolysis. This review will provide valuable guidance for the rational design of OER electrocatalysts, facilitating sustainable hydrogen production from seawater.

Dr. Daekyu Kim received his Ph.D. degree in material chemistry under the supervision of Prof. Lawrence Yoon Suk Lee at the Department of Applied Biology and Chemical Technology, the Hong Kong Polytechnic University (2024). He is currently working as a postdoctoral researcher at the Center for Hydrogen & Fuel Cell Research, the Korea Institute of Science and Technology (KIST). His research interests are mainly focused on the design of advanced nanomaterials for electrocatalytic water splitting and fuel cells.

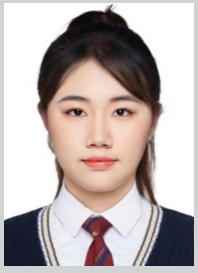

Wenhan ZU received her Bachelor's degree from Sun Yat-Sen University in 2023. She is currently pursuing her Ph.D. degree under the supervision of Prof. Lawrence Yoon Suk Lee at the Department of Applied Biology and Chemical Technology, the Hong Kong Polytechnic University. Her research interests include the development of novel nanomaterials based on transition metal complexes for electrocatalytic water splitting.

Ching Lam Kwok is an undergraduate student at the Department of Applied Biology and Chemical Technology, the Hong Kong Polytechnic University. Her research interests are covalent organic frameworks and single-atom catalysts for the oxygen reduction reaction. She is currently working on her final year project under the supervision of Prof. Lawrence Yoon Suk Lee.

Prof. Lawrence Yoon Suk Lee earned his Ph.D. degree in Chemistry from McGill University, Canada. He currently serves as an associate professor at the Department of Applied Biology and Chemical Technology, the Hong Kong Polytechnic University. His research interests are centered on understanding the atomic structure of nanomaterials for various photocatalytic and electrocatalytic processes, encompassing water splitting and CO_2 reduction, as well as advanced energy storage devices. His research group pioneers state-of-the-art characterization techniques such as in situ Raman, XRD, and operando TEM.

2. Fundamental of Water Electrolysis

2.1. Water Electrolysis in Alkaline Media

Water electrolysis involves two simultaneous half-reactions: the hydrogen evolution reaction (HER) at the cathode and the OER at the anode. These reactions occur *via* different reaction routes depending on the electrolyte conditions as follows:

The overall water electrolysis:

$$2H_2O \rightarrow O_2 + 2H_2,\ E^\circ = 1.23\ V \quad (1)$$

In acidic electrolytes:

$$\text{Cathode}:\ 4H^+ + 4e^- \rightarrow 2H_2,\ E^\circ = 0\ V \quad (2)$$

$$\text{Anode}:\ 2H_2O \rightarrow 4H^+ + O_2 + 4e^-,\ E^\circ = 1.23\ V \quad (3)$$

In alkaline electrolytes:

$$\text{Cathode}:\ 4H_2O + 4e^- \rightarrow 2H_2 + 4OH^-,\ E^\circ = -0.828\ V \quad (4)$$

$$\text{Anode}:\ 4OH^- \rightarrow 2H_2O + O_2 + 4e^-,\ E^\circ = 0.401\ V \quad (5)$$

Water electrolysis theoretically occurs at a potential of 1.23 V, as described in Equation 1. However, in practical water electrolysis, an additional energy known as overpotential (η) is required. This overpotential is necessary to overcome the kinetic barrier associated with the sluggish reactions of OER and HER. Given that the OER has slower kinetics compared to the HER, alkaline electrolysis typically exhibits higher efficiency than acidic electrolysis. This can be attributed to the fact that the OER, which is the major bottleneck in water electrolysis, proceeds more efficiently in alkaline media that are rich in OH^- ions.[34] The presence of OH^- ions facilitates the OER, reducing the overpotential required for the reaction to occur.

2.2. Mechanism and Challenges of Seawater Electrolysis

The presence of Ca^{2+} and Mg^{2+} in natural seawater can lead to the deposition of insoluble hydroxides with low solubility product values on the electrode surface, especially on the cathode surface. This deposition hinders charge transfer and poisons the active sites, thereby reducing the overall efficiency of the electrochemical reactions.[35] Na^+, which is abundant in seawater, can enhance the conductivity of the electrolyte without engaging in electrochemical reactions.[14] However, excess concentrations of Na^+ can cause fouling and corrosion of the electrode.[34] Furthermore, the complex chemical environment of seawater, which includes various inorganic ions, microorganisms, and small particles, can block and obstruct the electrode surface, leading to a decline in catalytic efficiency and stability.[13] In the anode, the presence of Cl^- is particularly problematic in seawater electrolysis. A high concentration of Cl^- can cause severe electrode erosion and react with electron-deficient transition metal ions during the reaction, resulting in the formation of low-demand ClO^- and Cl_2 species, as shown in the following equations:[13,16]

Chlorine evolution reaction (CER):

$$2Cl^- \rightarrow Cl_2 + 2e^-,\ E^\circ = 1.36\ V,\ pH = 0 \quad (6)$$

Hypochlorite formation reaction (HCFR):

$$Cl^- + 2OH^- \rightarrow ClO^- + H_2O + 2e^-,\ E^\circ = 0.89\ V,\ pH = 14 \quad (7)$$

The presence of chlorine and its associated reactions can compete with the OER, leading to a decrease in OER efficiency at the anode. Therefore, it is essential to enhance the selectivity of OER to address these challenges. In alkaline media, there is a significant potential gap of 480 mV between OER and the hypochlorite formation reaction (HCFR). This suggests that OER should ideally occur exclusively within this potential range (Figure 1). However, in practice, electrolysis under industrial standards, with current densities ranging from 500 to 1,000 mA cm^{-2} over extended periods of up to 60,000 hours, cannot completely avoid the HCFR, resulting in anode corrosion.[19] Furthermore, seawater typically has a near-neutral pH between 8.0 and 8.3.[34] Under these neutral conditions, the adsorption and dissociation of water molecules, which are the rate-determining step (RDS) in the seawater splitting process, face a high energy barrier, thereby slowing down the overall reaction kinetics.[34,36]

3. Interface Configurations

Interface engineering is a widely employed method to manipulate the electronic structure of electrocatalysts, with the aim of optimizing the charge transfer efficiency and binding interactions with OER intermediates.[20,23] In recent years, numerous OER electrocatalysts have been developed using various interface engineering strategies, such as heteroatom doping, chemical composition adjustments, morphology control, and amorphous/crystalline heterophase (Figure 2).[22,23,33,37–39] This section provides a summary of the different types of interface structures and their effects by examining the reported OER electrocatalysts in alkaline and seawater environments.

3.1. Doping

Doping is a simple and effective method used to tune the electronic structure of a material by incorporating foreign atoms into the host material.[25] The doped elements create the atomic interfaces with the host materials, exerting atomic-scale interface effects. Heteroatom doping effects encompass both metallic and non-metallic atom doping states.

To regulate the electronic structure of electrocatalysts and generate relevant vacancies, metallic atoms can be introduced into various metal composites. Li *et al.* incorporated V into NiFe layered double hydroxide (LDH) *via* a simple one-pot hydrothermal method.[40] Through Density functional theory (DFT)

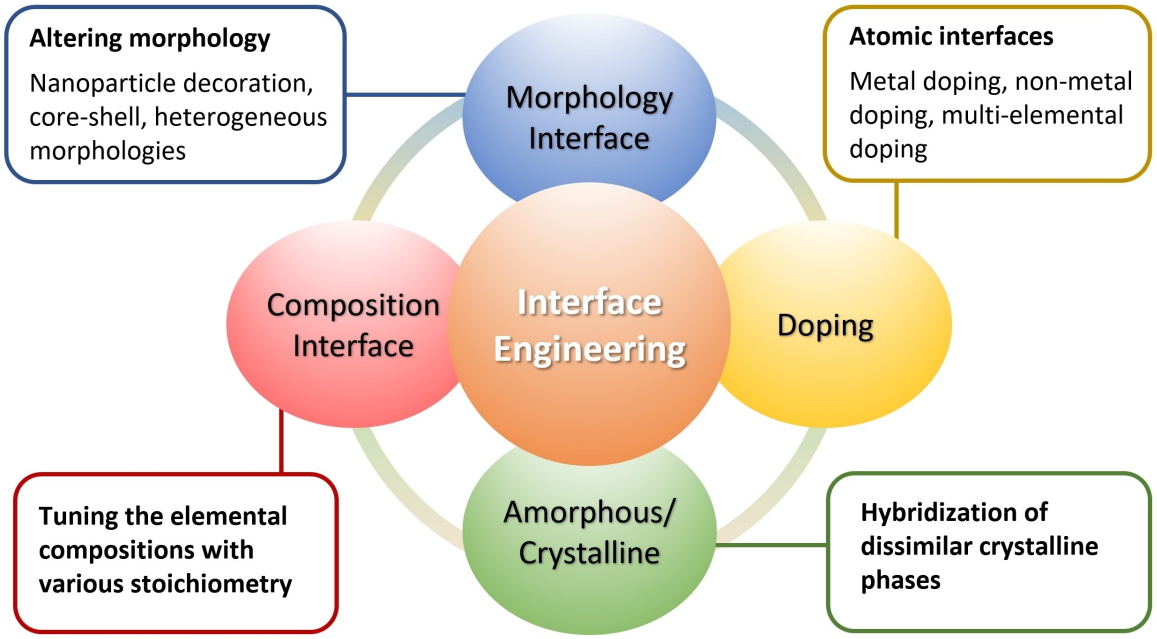

Figure 2. Types of interface configurations.

calculations and XPS analysis, it was demonstrated that V doping modified the electronic structure and shortened the bandgap of the catalyst, accelerating electron transfer, improving its conductivity, and creating numerous active sites. Consequently, the prepared catalysts exhibited excellent OER activity in alkaline conditions (1.0 M KOH). Rare earth elements have also been employed as dopants due to their rich electrons with empty 5*d* and 4*f* orbitals.[21,41] For example, Li *et al.* prepared Gd-doped NiFe LDH using a straightforward one-pot hydrothermal process (Figure 3a).[41] Gd doping was found to tune the electronic structures of elements within NiFe LDH, specifically enhancing the density of states associated with exposed Ni (Figures 3b–e). This manipulation facilitated the generation of HOO* on the Ni active site (Figure 3f), leading to improved OER activity and stability of the NiFe LDH catalyst (Figure 3g). Furthermore, studies have also been conducted on metal doping-based catalysts for highly active seawater oxidation. Luo *et al.* synthesized an Mn-doped Ni_2P/Fe_2P through hydrothermal and phosphating treatments, demonstrating its excellent OER performance in simulated seawater.[42] Mn doping effectively modulated the electronic structures of Fe and Ni within Ni–Fe phosphide, leading to the creation of additional active sites. This, combined with the inherent corrosion resistance of Ni–Fe phosphide, resulted in impressive OER performance. The catalyst exhibited a low overpotential of 358 mV at a high current density of 1,000 mA cm^{-2} and maintained this performance for an extended period of 200 h in simulated seawater. Additionally, Zhang *et al.* revealed that high-valence Cr dopant could effectively regulate the electronic structures and reinforce the corrosion resistance of the cobalt carbonate hydroxide nanowire array, resulting in outstanding OER performance in alkaline solution and simulated seawater.[43]

In addition to metallic elements, non-metal elements can also be doped into electrocatalysts to regulate the electronic structures, tune valence states, and optimize energy barriers. Non-metal doping can be achieved by various simple treatments, including hydrothermal reaction, one-pot solution-phase method,[44] and molten salt process.[45] For instance, Niu *et al.* synthesized Se-doped FeOOH *via in situ* electrochemical oxidation based on hydrothermal treatment.[46] DFT studies showed that Se doping significantly reduced the energy barrier of the RDS for the transition from M–O to M–OOH species. As a result, Se-doped FeOOH showed an exceptional performance with an overpotential of 348 mV at a high current density of 500 mA cm^{-2} in 1.0 M KOH. Chen *et al.* synthesized a S-doped NiFe LDH catalyst and demonstrated the effect of S doping on the complete reconstruction process.[47] Intriguingly, the initially doped sulfur elements leached out during the process, facilitating the reconstruction of the material into highly active Ni–FeOOH. This reconstruction activated lattice oxygen redox reactivity, leading to exceptional OER performance. The resulting Ni–FeOOH catalyst exhibited a low overpotential of 224 mV at 100 mA cm^{-2}, while maintaining stability for 150 hours under stepwise current density conditions. The enhanced OER performance achieved by non-metallic doping was also confirmed in simulated seawater electrolytes. Song *et al.* improved the OER activity of NiFe LDH through P doping, while adjusting the P doping concentrations.[48] P doping was found to improve OER activity and stability by preventing anion and cation leaching from NiFe LDH and promoting the production of high-valent Ni^{4+} species (Figures 4a–f). The study further revealed that interstitial P doping shifted the RDS from the second (*O→ *OOH) to the third (OOH→O_2) step, consequently reducing the reaction barrier at the RDS. This manipulation resulted in enhanced OER catalysis and reduced the involvement of Cl^-

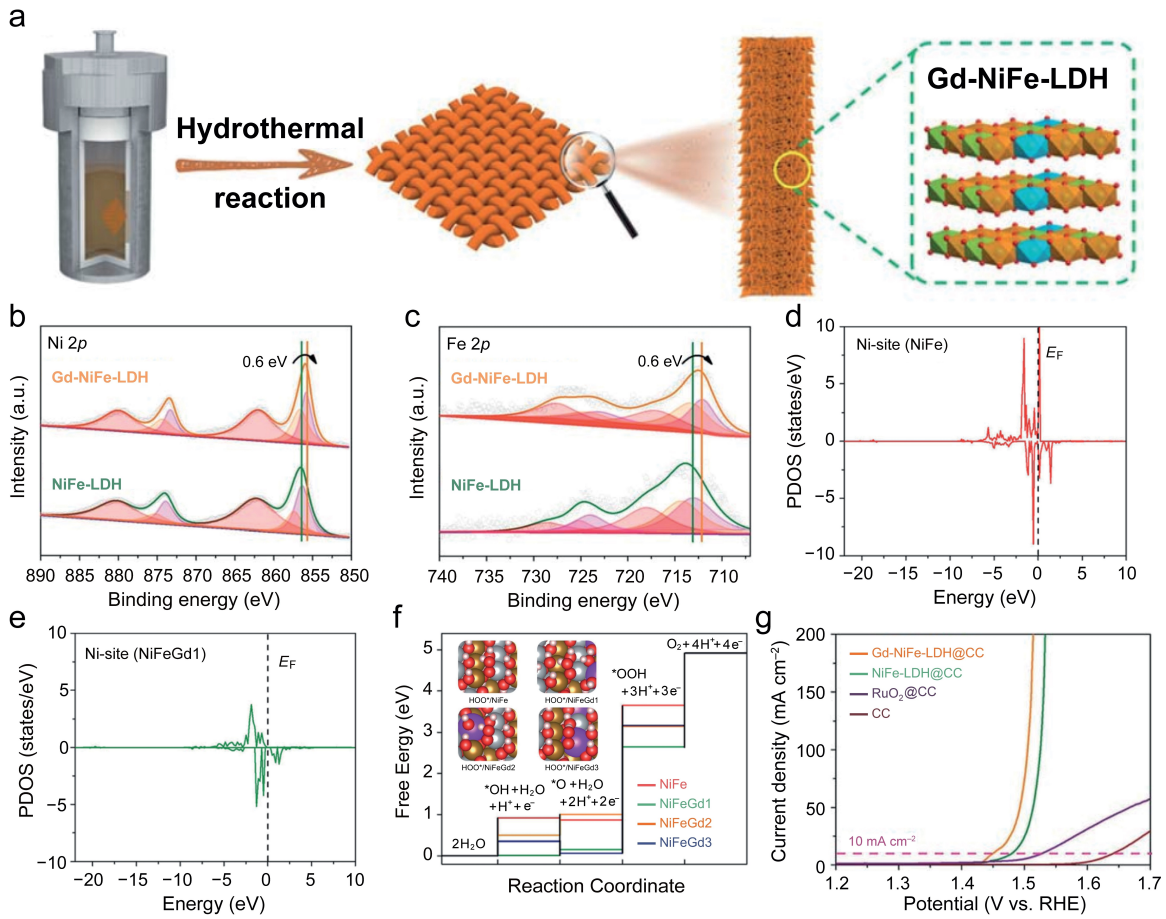

Figure 3. (a) Synthetic procedure for Gd-NiFe-LDH. High-resolution (b) Ni 2*p* and (c) Fe 2*p* XPS spectra of Gd-NiFe-LDH and NiFe-LDH, respectively. Calculated projected density of states of the Ni sites on (d) NiFe and (e) Gd-doped NiFe. (f) Gibbs free energy diagram for OER on NiFe and Gd-doped NiFe LDH. (g) LSV curves of Gd-NiFe-LDH and control samples on carbon cloth. Inset in (f) illustrates the HOO* adsorption configurations on the surface of NiFe and three different Gd-doped NiFe models. Pink, red, grey, brown, and purple spheres indicate H, O, Ni, Fe, and Gd, respectively. Reproduced with permission.[41] Copyright 2021, Royal Society of Chemistry.

ions. Benefiting from this P doping, a promising OER performance was achieved in both simulated seawater (1.0 M KOH + 0.6 M NaCl) and natural seawater, as illustrated in Figures 4g–i.

Doping multiple elements into a catalyst can have a significant impact on improving its performance due to the synergistic effect of various elements. Jiang *et al.* developed Fe and V co-doped nickel (oxy)hydroxide ($Ni_3Fe_{0.5}V_{0.5}$) nanosheets on carbon fiber paper.[49] The introduction of Fe and V atoms induced their synergistic interaction with the host nickel (oxy)hydroxide, leading to improved OER activity by affecting the electronic structures and local coordination environments. Intriguingly, their study revealed a contraction of V–O bonds in $Ni_3Fe_{0.5}V_{0.5}$ during the OER process, leading to the formation of high-valent V species close to the 5+ oxidation state. These high-valent V sites exhibited optimal binding interactions with reaction intermediates compared to Ni and Fe sites. Consequently, $Ni_3Fe_{0.5}V_{0.5}$ demonstrated superior OER performance compared to the undoped sample, achieving a lower overpotential of 291 mV at 500 mA cm^{-2} and stable catalysis for 60 h under 100 mA cm^{-2} in 1.0 M KOH. In another study conducted by Chang *et al.* Fe and P-co-doped $NiSe_2$ nanofilms (Fe, P–$NiSe_2$ NFs) were fabricated through electrodeposition and phosphating.[50] It was confirmed that the Fe dopant increased the selectivity of the OER intermediate, while P suppressed the dissolution of Se by creating a P–O layer. Owing to the synergistic effects of the co-doping, the electrolyzer constructed using Fe, P–$NiSe_2$ NFs required a low cell voltage of 1.8 V to achieve a current density of 0.8 A cm^{-2} and exhibited stable performance for 200 h in natural seawater.

These exceptional performances emphasize that doping creates atomic interfaces within host materials, which significantly impact the electronic structures, atomic arrangements, and bonding nature. By strategically selecting dopants and employing effective doping techniques, the binding energies of OER intermediates can be optimized, resulting in enhanced activity and selectivity toward the OER process. This improved activity and selectivity have the potential to enable electrocatalysts to sustain OER over extended periods without interference from competing CER in seawater. In addition to doping strategies, the incorporation of anti-chlorine corrosion elements such as Cr and P presents an effective approach to prevent the disintegration of active species from the catalysts in seawater environments. These anti-corrosion elements help to maintain the structural integrity and stability of the catalysts,

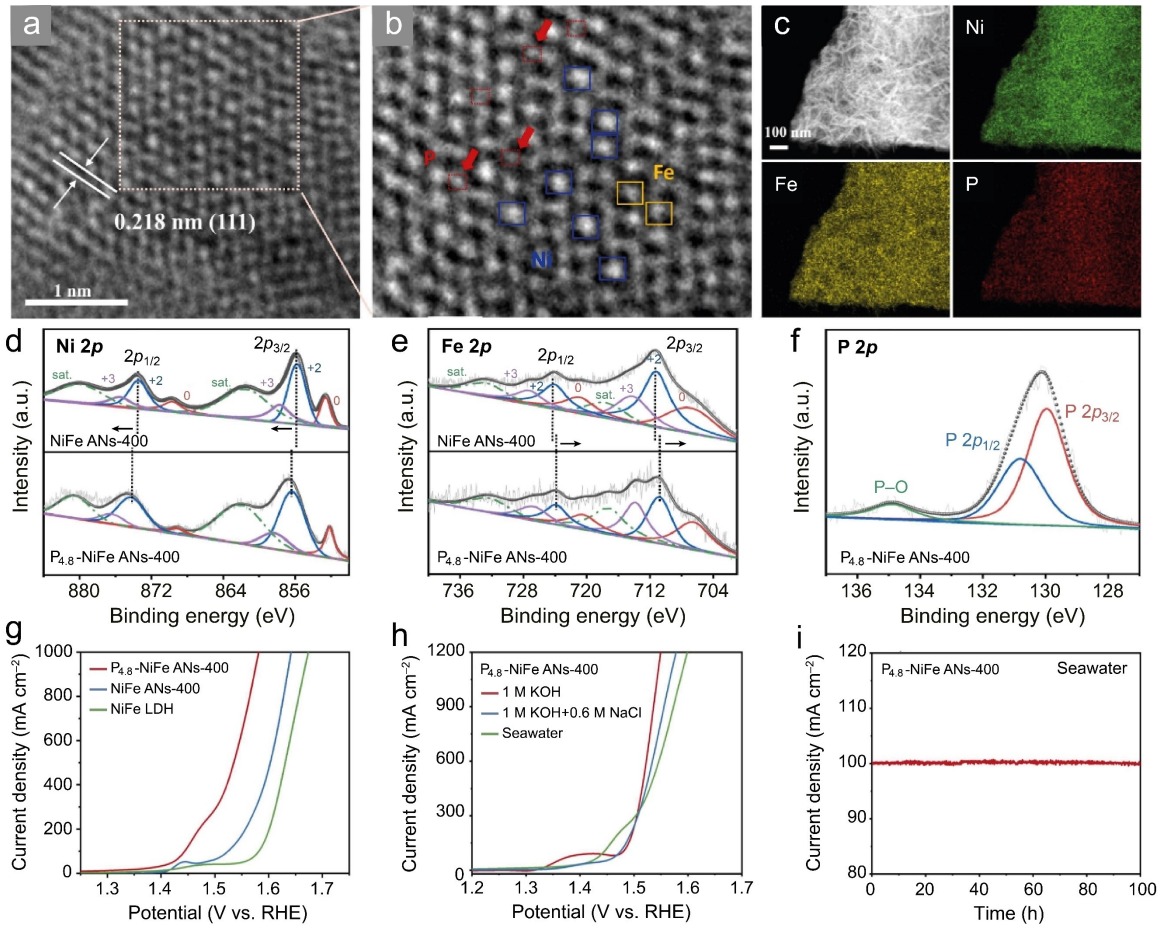

Figure 4. (a,b) HRTEM and (c) EDX mapping images of $P_{4.8}$-NiFe ANs-400. High-resolution (d) Ni 2*p*, (e) Fe 2*p*, and (f) P 2*p* XPS spectra of NiFe ANs-400 and $P_{4.8}$-NiFe ANs-400. (g) LSV curves of $P_{4.8}$-NiFe ANs-400 and control samples in simulated seawater (1.0 M KOH + 0.6 M NaCl). (h) LSV curves of $P_{4.8}$-NiFe ANs-400 in various electrolytes. (i) *I*-t curve of $P_{4.8}$-NiFe ANs-400 in seawater. Reproduced with permission.[48] Copyright 2024, Elsevier.

enabling long-term OER catalysis in the presence of chlorine-containing species.

3.2. Compositional Interface

Compositional interfaces are formed within a single material by varying the elemental composition stoichiometrically. These interfaces can facilitate electron transfer by creating favorable electronic pathways. This can potentially lead to several benefits, such as reducing the energy required for the RDS of the OER and promoting the formation of abundant active sites. Mu *et al.* designed heterostructures composed of Mo-doped Ni_3S_2 and nickel phosphide (Mo–Ni_3S_2/Ni_xP_y/NF) by a solvothermal process followed by phosphorization.[51] This Mo- and P-doped heterostructure synergistically optimized the Gibbs free energies of H- and O-containing intermediates (OH*, O*, and OOH*). The introduction of Mo and P increased the positive and negative charge states (δ^+/δ^-) in Ni and S sites, respectively, compared to pristine Ni_3S_2 due to strong electronic interactions between the multiple components. This optimized electronic structure configuration facilitated efficient electron transfer, leading to enhanced OER activity in 1.0 M KOH. The catalyst exhibited a low overpotential of 238 mV at 50 mA cm^{-2}. Notably, the stability of the catalyst was excellent with no degradation observed during chronopotentiometry measurement at 20 mA cm^{-2} for 30 h. Additionally, the catalyst maintained its morphology, crystalline structure, and electronic structure throughout the long-term stability test. Yang *et al.* reported the *in situ* growth of a 3D hierarchical Ni_3S_2/VS_4 nanohorn array on nickel foam through a one-step solvothermal reaction.[52] The exceptional OER performance of the catalyst, achieving 317 mV at 50 mA cm^{-2} and maintaining stability for 20 h in 1.0 M KOH, was attributed to the presence of V^{4+} in VS_4. This V^{4+} species exhibits a strong affinity for oxygen atoms, promoting efficient OER catalysis. Partial leaching of VS_4 resulted in the facile formation of a surface with abundant nickel oxide sites, which acted as an active site for the OER. Ultimately, this enhanced the selectivity with oxygenic intermediates namely, increased adsorption OH^-, and accelerated the RDS in OER. Tang *et al.* synthesized heterogeneous bimetallic Mo–NiP_x/NiS_y nanowires through phosphorization and sulfuration.[53] The Mo–NiP_x/NiS_y nanowires consisted of heterogeneous interfaces of Ni_2S_3 with various components such as $Ni_{12}P_5$, Ni_2P, and $Ni_{17}S_{18}$ (Figures 5a–g). This unique interfacial configuration enhanced the chemical adsorption

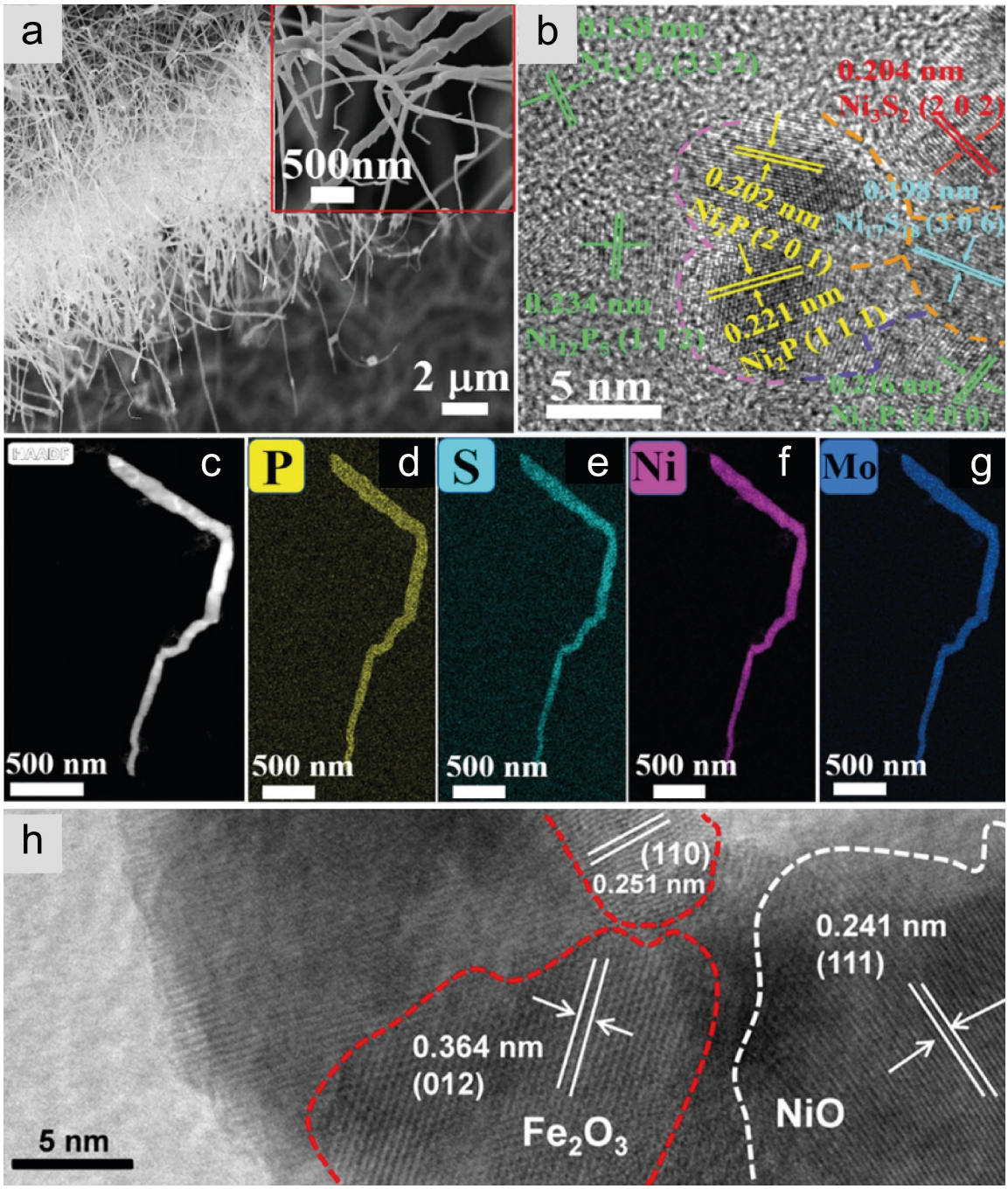

Figure 5. (a) SEM, (b) HRTEM, and (c–g) EDS mapping images of Mo-NiP_x/NiS_y nanowire. Dotted lines in (b) indicate heterogeneous interfaces among the components. Reproduced with permission.[53] Copyright 2021, Wiley-VCH. (h) HRTEM image of FNE 300. Reproduced with permission.[56] Copyright 2021, American Chemical Society.

capacity and modified the electron distribution to active sites, resulting in remarkable OER performance in 1.0 M KOH.

Catalysts with compositional interfaces have also demonstrated excellent OER performances in seawater electrolytes. Yu *et al.* prepared interconnected nanosheets of Fe_2P/Ni_3N using a multi-step approach.[54] Initially, thermal nitridation was applied to Ni foam soaked in acetic acid, followed by immersion in a solution containing Fe and Co precursors and subsequent phosphorization. The strong electronic interactions and unique interconnected nanostructure of Fe_2P/Ni_3N facilitated the charge transfer, mass transport, and provided numerous active sites and efficient release of gas bubbles. Consequently, Fe_2P/Ni_3N demonstrated a low overpotential of 302 mV at a high current density of 500 mA cm^{-2} in 1.0 M KOH + seawater. Furthermore, the catalyst exhibited remarkable resistance to corrosion even under industrially relevant current densities. This exceptional stability is attributed to the *in situ* generation of high valent Fe, Ni, nitrate, and phosphate species at the catalyst

surface during OER in seawater. This transformation effectively prevents chloride corrosion of the underlying metallic Ni foam, ensuring long-term stability. Zhou *et al.* designed a self-supported $Fe_2P/Ni_{1.5}Co_{1.5}N/N_2P$ heterostructure array through a two-step process.[55] Fe_2P was first grown on the surface of nickel cobalt nitride, followed by Fe modification and phosphorization. The resulting interfaces between these components exhibited synergistic properties, including high conductivity, facilitating water adsorption and dissociation, and enhanced adsorption of hydrogen and oxygenated species. Such effects led to high performances in 1.0 M KOH + seawater electrolyte. The RDS for Fe sites on $Fe_2P/Ni_{1.5}Co_{1.5}N$ was the third step for the conversion of *O to *OOH and required much less energy compared to its individual components. This behavior may be attributed to strong electronic interaction between components, facilitating electron transfer. Ultimately, this catalyst demonstrated OER performance with low overpotentials of 255 and 307 mV at current densities of 100 and 500 mA cm^{-2}, respectively, in a 1.0 M KOH + seawater electrolyte. DFT calculations revealed that the catalyst exhibited high selectivity for OER in seawater due to a lower OH^- adsorption energy compared to Cl^-, promoting the desired reaction pathway. Furthermore, the transformation of P species to higher valence states during OER served as an effective protection mechanism against chloride corrosion on the underlying Ni foam. Yang *et al.* prepared an electrocatalyst named FNE300, which consists of a Fe_2O_3/NiO layer on a nickel foam substrate.[56] It was synthesized using a scalable dipping-and-heating method. This approach facilitated the growth of a well-defined interface between NiO and Fe_2O_3, optimizing the electronic structure and promoting efficient intermediate adsorption (Figure 5h). Additionally, the repulsion between Ni^{2+} and oxygen intermediates (e^-–e^- repulsion) further enhanced the interaction between Fe and oxygenated intermediates. Additionally, the layer of oxygenated intermediates attached to the catalyst's surface and its porous structure allowed for the efficient release of oxygen. These synergistic effects resulted in an impressive overpotential of 291 mV at a high current density of 1,000 mA cm^{-2} in an electrolyte consisting of 1.0 M KOH mixed with seawater. Besides, the FNE300 exhibited good stability in alkaline domestic sewage, even at high chemical oxygen demand levels, after 20 hours of testing at around 50 mA cm^{-2}.

Our review of the studies reveals that compositional interfacial configuration plays a crucial role in tuning the Gibbs free energy of reaction intermediates, influencing their adsorption ability and enabling selective promotion of the OER. Notably, the composition of some catalysts can evolve to higher valence states, forming a protective film that effectively combats chloride corrosion, a critical attribute for seawater applications.

3.3. Morphological Interface

The strategic design of a catalyst's morphology plays a crucial role in enhancing its electrocatalytic performance.[57] One strategy involves the creation of morphological interfaces, which are formed by combining components with different morphologies within a single material. These interfaces can be broadly categorized into three types: 1) particles on the substrate, 2) core–shell structure, and 3) heterogeneous morphological structure. Particles on substrate type consists of active nanoparticle species (0D) deposited onto higher dimensional structures such as 1D nanowires, 2D nanosheets, and 3D nanostructures. This configuration offers a high density of active sites due to the nanoparticles, potentially leading to improved catalytic activity.[58–61] Hu *et al.* designed a heterostructure composed of NiFe LDH/NiTe by the partial chemical etching of nickel foam, followed by a hydrothermal process to deposit NiFe LDH.[62] This innovative design effectively created intimate interfaces between NiFe LDH and NiTe (Figures 6a–b), thereby reducing the binding strength of intermediates. The electron transfer from NiTe to NiFeOOH at the interface resulted in the accumulation of electrons on the NiFeOOH side (Figures 6c–d). Furthermore, the free energy profiles indicated that the modifications to the adsorption of intermediates on the interface led to a reduction in the energy barrier of the RDS. Notably, this heterostructure achieved an impressive OER performance in 1.0 M KOH, with an overpotential of 228 mV at 50 mA cm^{-2} and catalytic stability for 30 h under 20 mA cm^{-2}.

Core–shell structure refers to the composites consisting of a core material surrounded by a shell of a different material. This design can improve stability, conductivity, and selectivity by optimizing the properties of each component. Wang *et al.* successfully prepared three-dimensional core–shell heterostructured $Ni_xS_y@MnO_xH_y$ nanorods on nickel foam using a hydrothermal reaction followed by an electrodeposition process.[63] The catalyst exhibited overpotentials of 326 and 356 mV at current densities of 100 and 500 mA cm^{-2}, respectively, in 1.0 M KOH. The abundant active sites facilitated mass transport and the diffusion of bubbles, while the synergistic effect between MnO_xH_y and Ni_xS_y reduced charge-transfer resistance, demonstrating improved reaction kinetics for OER. Furthermore, MnO_xH_y shell acted as protective layers, inhibiting electrochemical corrosion which occurs at high anodic potentials. Owing to the MnO_xH_y protective shell, $Ni_xS_y@MnO_xH_y$ showed stable OER catalysis for 100 h under 100 mA cm^{-2}, which outperformed the pristine Ni_xS_y.

Heterogeneous morphological structures encompass various complex morphologies combining different materials and structures, forming interfacial domains to achieve synergistic effects for enhanced performance. Li *et al.* fabricated a hybrid catalyst, CoFeO@BP, by growing amorphous cobalt and iron oxide on two-dimensional black phosphorus (BP) using a one-step solvothermal method.[64] The amorphous structure of the catalyst played a crucial role in facilitating the oxidation of Co^{2+} to Co^{3+} and created abundant active sites for promoted adsorption of hydroxyl species and facilitated participation of lattice oxygen. The strong affinity between BP and transition-metal ions promoted a uniform growth of amorphous CoFe oxide on the surface, activating lattice oxygen and catalyzing the OER through the lattice oxygen-mediated (LOM) mechanism. As a result, the distinctive structured CoFeO@BP could

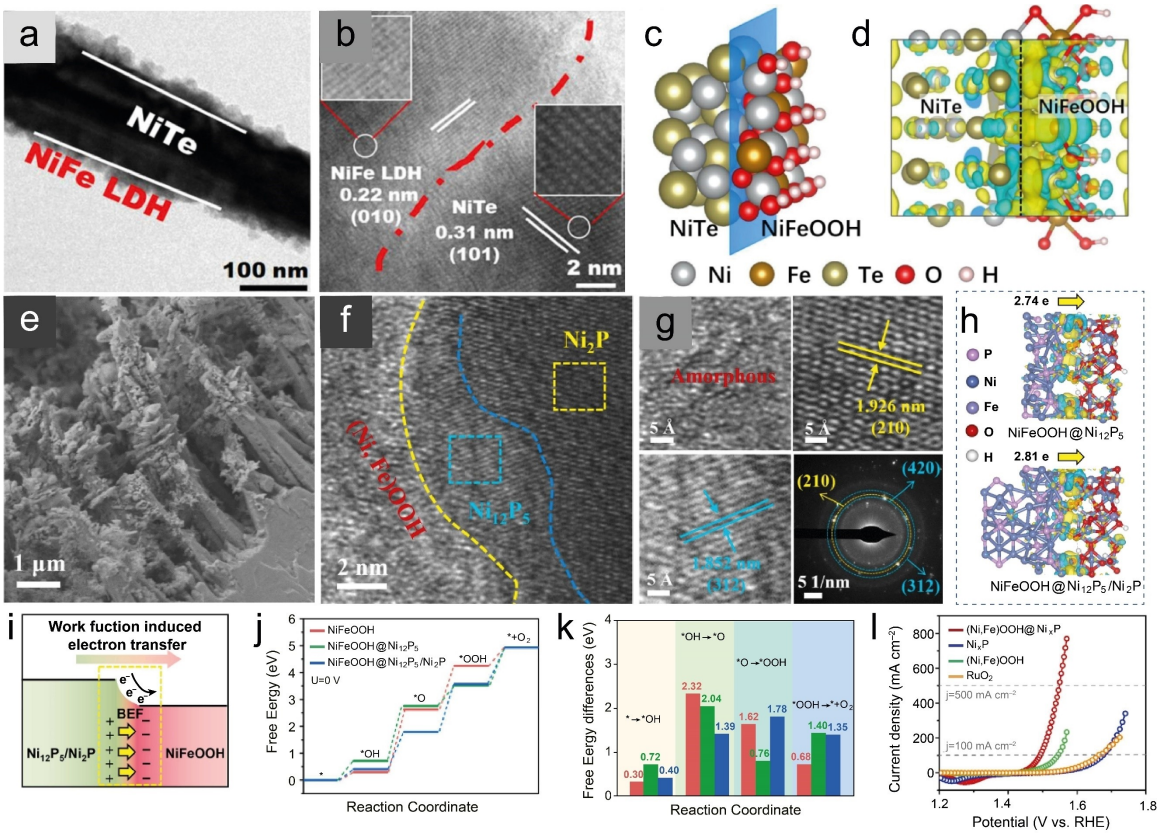

Figure 6. (a) TEM and (b) HRTEM images of NiFe LDH/NiTe. (c) Simulated NiFe LDH/NiTe structure and (d) charge density differences at the interfaces. Yellow and blue regions indicate electron accumulation and depletion areas, respectively. Reproduced with permission.[62] Copyright 2020, Elsevier. (e) SEM, (f) HRTEM, and (g) the corresponding enlarged images of (Ni, Fe)OOH@$Ni_{12}P_5$/Ni_2P. (h) Charge density differences of (Ni, Fe)OOH@$Ni_{12}P_5$ and (Ni, Fe)OOH@$Ni_{12}P_5$/Ni_2P. (i) Charge transfer process at the interface between NiFeOOH and $Ni_{12}P_5$/Ni_2P. (j) OER pathway and (k) the corresponding free energy differences at each reaction step of samples. (l) LSV curves of (Ni, Fe)OOH@$Ni_{12}P_5$/Ni_2P and control samples in alkaline natural seawater. Reproduced with permission.[66] Copyright 2023, Elsevier.

deliver a current density of 10 mA cm^{-2} for 24 h at an overpotential of 266 mV in 1.0 M KOH.

Morphology interface-modified catalysts also have demonstrated favorable OER performance in seawater electrolytes. Cong *et al.* fabricated a $Co_{0.4}Ni_{1.6}P$–CeO_2/NF catalyst by depositing CeO_2 nanoparticles onto the surface of metal–organic frameworks (MOF)-derived $Co_{0.4}Ni_{1.6}P$ nanowire arrays.[65] The synthetic process involved subjecting a nickel foam to hydrothermal treatment, followed by immersion in 2-methylimidazole and another round of hydrothermal treatment for phosphorization. The introduction of CeO_2 nanoparticles, which are known to have anti-corrosion abilities, played a crucial role in maintaining the structural integrity and thus stability of the catalyst. The synergistic effect between CeO_2 and $Co_{0.4}Ni_{1.6}P$ resulted in multiple benefits, including an abundant exposed active area, redistribution of charge at the interface, and generation of rich oxygen vacancies, thereby enhancing the charge-transfer ability. The catalyst exhibited overpotentials of 268 and 343 mV at 10 and 100 mA cm^{-2}, respectively, in 1.0 M KOH. In simulated alkaline seawater, it demonstrated an overpotential of 345 mV at 100 mA cm^{-2}. Additionally, the $Co_{0.4}Ni_{1.6}P$–CeO_2/NF catalyst exhibited superior stability compared to the $Co_{0.4}Ni_{1.6}P$/NF catalyst, due to the presence of CeO_2 nanoparticles. Zhang *et al.* presented a heterogeneous catalyst, (Ni, Fe)OOH@Ni_xP, which contained a dual interface composed of (Ni, Fe)OOH/$Ni_{12}P_5$/Ni_2P (Figures 6e–g).[66] At the interface between the $Ni_{12}P_5$/Ni_2P and (Ni, Fe)OOH, an asymmetric charge redistribution occurred, forming a spontaneous built-in electric field (BEF, Figures 6h–i). This electric field facilitated the adsorption kinetics of oxygenic intermediates and electron transfer. Consequently, the free energy required for the RDS (*O→*OOH) was minimized (Figures 6j–k). The dual-interface configuration enhanced the BEF and weakened Cl^- adsorption, partially impeding the COR process. Also, the particle-nanowire of (Ni, Fe)OOH@Ni_xP possessed the superoleophobicity, which was beneficial for the transport of electrolyte and gas products, leading to excellent OER performance in 1.0 M KOH + seawater electrolyte (Figure 6l). Bao *et al.* addressed the low conductivity of the OER-active but less conductive Fe-BDC by constructing a heterostructure with p-type $CoWO_4$.[67] This organic–inorganic junction facilitated electronic structure modulations, generating high-valent Co^{3+} and oxygen vacancies, redistributing the charge density, which optimized interactions with OER intermediates. Consequently, Fe-BDC/$CoWO_4$ exhibited remarkable OER activity and stability in alkaline media, achieving an overpotential of 290 mV at 100 mA cm^{-2} and maintaining

activity for 250 h in simulated seawater, demonstrating its effectiveness in preventing chlorine evolution. Li *et al.* designed a heterostructure catalyst based on bimetallic nitrides and nickel tellurides on a core–shell nanorod array (NiTe–NiFeN) using a hydrothermal method, followed by an *in situ* electrochemical deposition and subsequent nitridation.[68] The synergistic effect between the NiFeN and NiTe at the interface modulated the electronic structures, leading to the modification of adsorption properties for the reaction intermediates and optimization of the energy barrier for the RDS. Besides, the nanoarray structure exposed numerous active sites in the bimetallic nitride shell, facilitating rapid electron and mass transportation and achieving high wettability. Moreover, the core–shell structure, with nanosheet wrapping, fully mobilized the active sites within the catalyst, enhancing the local electric field strength and thus creating a hydroxide-rich area, which improved OER kinetics and retarded the CER. Owing to those features, the NiTe–NiFeN exhibited an overpotential of 211 mV at 10 mA cm^{-2} and 40 h of stable catalysis in 1.0 M KOH. It also demonstrated seawater splitting using an electrolytic cell coupled with NiTe–NiCoN in 1.0 M KOH + seawater. The electrolytic cell required a cell voltage of 1.84 V to deliver a current density of 400 mA cm^{-2} and could operate 100 h with no significant degradation under 100 mA cm^{-2}.

A proper design of morphological interfaces offers a trifecta of benefits: excellent stability, rapid electron–mass transport, and high wettability. These properties make them ideally suited for long-term commercial applications. As discussed in this section, the formation of an interface structure involving a material with Cl^- passivation and oxygen permeation capabilities can significantly improve the catalytic durability in seawater. This combination of properties helps to mitigate degradation and maintain the structural integrity of the catalyst under corrosive conditions. Alternatively, by tuning the local electric field through morphological control, it is possible to create an interface that promotes the enrichment of OH^- ions on the catalyst surface. This enrichment can enhance the formation of protective passivating layers, contributing to improved durability in seawater. Additionally, the construction of these interfaces can influence selectivity towards the OER, which is crucial for effective utilization of catalysts in seawater environments.

3.4. Amorphous/Crystalline Heterophase

Amorphous materials have gained attention in electrocatalysis due to their high intrinsic activity, attributed to their disordered arrangement and unsaturated coordination structure that can create a large number of active sites.[38,69] However, they often suffer from low conductivity and structural instability. On the other hand, crystalline materials exhibit usually better electronic conductivity and catalytic stability but lack sufficient catalytic activity due to the absence of unsaturated bonds and active sites.[70] To address these limitations, researchers have sought to combine the advantages of both amorphous and crystalline structures, leading to the development of amorphous/crystalline heterostructures. Various methods have been employed to prepare these heterostructures, including hydrothermal method,[70–76] water bath method,[77] oil bath method,[78] solvent thermal method,[79] electrodeposition method,[80] and aged method.[81] By synthesizing amorphous/crystalline structures, the characteristics of multiple active sites and high conductivity associated with the amorphous and crystalline phases, respectively, can be retained. Moreover, the synergistic effect between the two structures can optimize the adsorption and desorption of intermediates and facilitate rapid electron transfer.

Dutta *et al.* employed the thermal deposition method to create an amorphous/crystalline mixed-phase catalyst with a core–shell structure consisting of crystalline Fe_3O_4 and amorphous Ni_xP.[82] The presence of crystalline Fe_3O_4 in the core enabled the formation of an amorphous Ni_xP shell, forming the amorphous-crystalline interface. Such interfacial structure increased electronic conductivity. Moreover, Fe species in the core Fe_3O_4 activated Ni by partial electron shifts, enabling the redox process from Ni^{3+} to Ni^{4+}, resulting in enhanced OER activity. Kuang *et al.* utilized the oil bath method and subsequent cation exchange process to form an amorphous/crystalline heterogeneous interface in cobalt-vanadium-iron (oxy)hydroxide (CoV–$Fe_{0.28}$).[83] Incorporating Fe ions turned out a key role in creating amorphous/crystalline structures by replacing Co ions and regulated electronic structures through the electronic interplays among Fe, Co, and V *via* oxygen bridge, strengthening the delocalization of π-symmetry electrons in the structure. Such effects generated electron deficient Co, Fe species, increasing the electronic conductivity and optimizing the adsorption of OER intermediates. In addition, the amorphous/crystalline structures by incorporation of Fe ions induced structural distortions including surface defects and dangling bonds, ensuring the structural durability and numerous exposed active sites. As a result, the CoV–$Fe_{0.28}$ required a low overpotential of 215 mV to reach 10 mA cm^{-2} and exhibited stable OER catalysis for 40 h at a fixed potential of 1.55 V in 1.0 M KOH. Singh *et al.* combined the crystalline phase V–Co_4N and the amorphous phase $CoNiPO_x$ ($CoNiPO_x$@V–Co_4/NF) through hydrothermal treatment, subsequent nitridation, and cyclic voltammetry (CV, Figure 7a).[84] The synergetic effects arising from V doping and amorphous–crystal interface interactions increased the density of states near the Fermi level and optimized the binding strength with OER intermediates (Figures 7b–e). This optimized catalyst demonstrated excellent OER performance in alkaline media.

OER catalysts with amorphous/crystalline interface have also been engaged in seawater oxidation. For example, Du *et al.* investigated the OER performance of a catalyst composed of crystalline Ru phase and amorphous Ni(Fe)P_2 phase in an alkaline solution and seawater.[85] Interfaces formed between Ru nanocrystals and amorphous Ni(Fe)P_2 facilitated charge accumulation, leading to enhanced electronic conductivity and reduced the energy barrier at the RDS (OH* formation) (Figures 7f–h). The synthesized Ru–Ni(Fe)P_2 required 375 and 520 mV to achieve a high current density of 1,000 mA cm^{-2} in 1.0 M KOH and seawater, respectively. Zhang *et al.* synthesized a heterostructure consisting of crystalline Ni_2P, Fe_2P, CeO_2, and

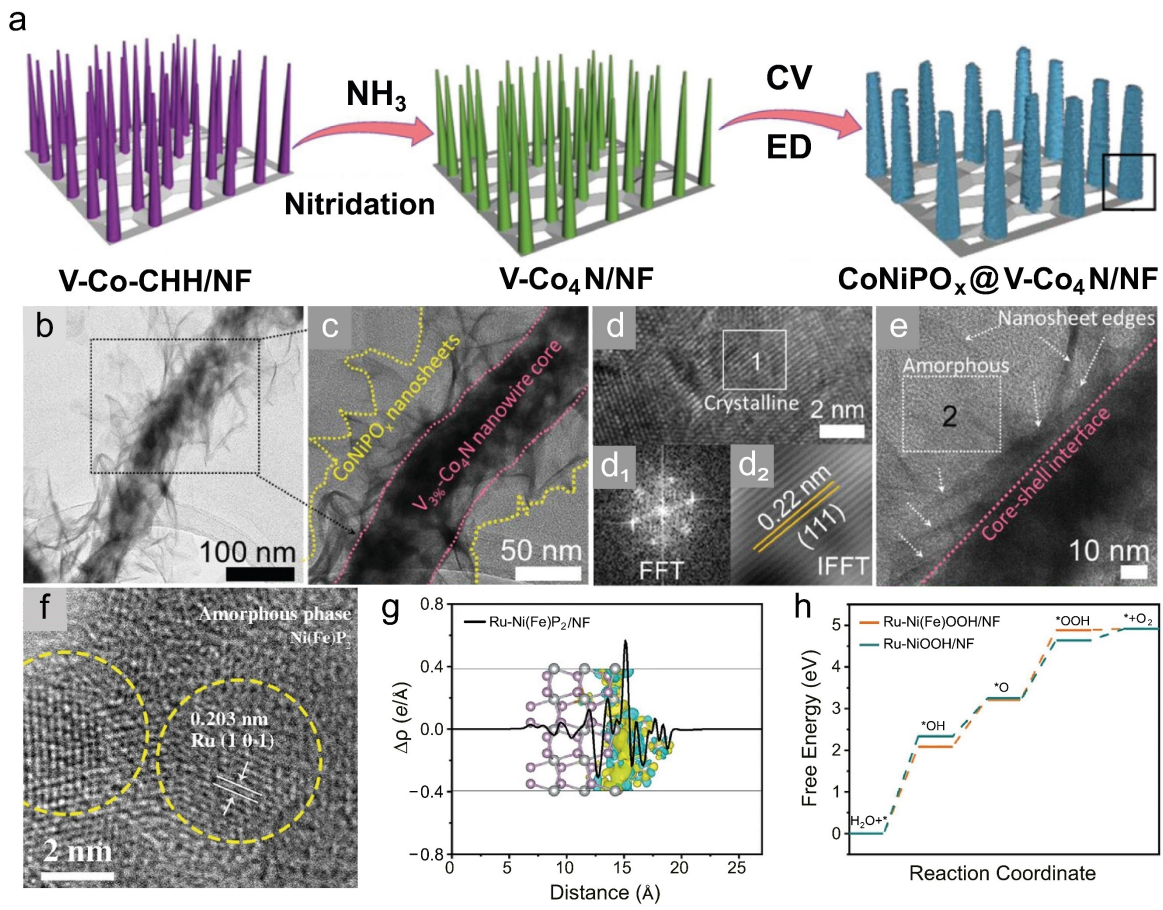

Figure 7. (a) Schematic illustrating the synthetic procedure, (b) TEM, and (c) HRTEM images of amorphous–crystalline $CoNiPO_x$@V–Co_4N/NF. HRTEM images of (d) crystalline core V–Co_4N and (e) amorphous shell $CoNiPO_x$. Reproduced with permission.[84] Copyright 2022, Wiley-VCH. (f) HRTEM image of Ru–Ni(Fe)P_2 composed of Ru nanocrystals and amorphous Ni(Fe)P_2. (g) Charge density distribution of Ru–Ni(Fe)P_2. (h) OER pathways of Ru–Ni(Fe)OOH and Ru-NiOOH. Reproduced with permission.[85] Copyright 2023, Wiley-VCH.

amorphous NiFeCe oxide on Nickel foam (NiFeO–CeO_2/NF) using a four-step solvothermal–cation exchange–phosphorization–CV treatment.[86] Numerous tiny crystalline nanoparticles ranging between 5 and 10 nm anchored on amorphous NiFeCe nanosheet structure provided a roughened surface with dense active sites, endowing the superhydrophilicity. Additionally, the high density of interfacial domains regulated the spatial charge distribution to generate highly active Ni species and increased charge transfer rate. Thus, NiFeO–CeO_2/NF required only an overpotential of 290 mV to reach the 1000 mA cm^{-2} and maintained catalytic activity for 200 h in 1.0 M KOH. DFT calculations revealed that the amorphous–crystalline interfaces remarkably increased the number of density of states, increasing the electrical conductivity. Moreover, such interface configuration of NiFeO–CeO_2/NF effectively reduced the transition energy from *O to *OOH. The activity of NiFeO–CeO_2/NF in alkaline media was good enough to avoid the formation of hypochlorite, exhibiting high current density OER performance in alkaline seawater.[86]

In summary, amorphous/crystalline heterophase structures offer a promising approach for designing OER catalysts. This strategy combines the high conductivity and stability of crystalline materials with the abundant active sites of amorphous materials. As reviewed in this section, catalysts with this heterophase structure exhibit improved catalytic activity, stability, and optimized adsorption/desorption energies of reaction intermediates. In the context of seawater environments, the optimized selectivity towards OER intermediates achieved through the heterophase structure can play a crucial role in improving catalytic durability. By favoring the desirable OER intermediates, the catalyst can effectively prevent the adsorption of Cl^- ions on the catalytic surface, thereby mitigating the detrimental effects of Cl^- adsorption and corrosion. This, in turn, enhances the overall stability and longevity of the catalyst in seawater. The presence of amorphous/crystalline interface domains can further amplify these effects. This is achieved by the redistribution of charge and modulation of electronic structures between the amorphous and crystalline phases. Additionally, defects generated at the interface, such as vacancies, dislocations, and stacking faults, can act as additional active sites and further improve OER reaction kinetics.

4. Conclusions and Perspectives

Seawater splitting is an attractive method for sustainable hydrogen production due to its economic and environmental benefits. However, the presence of impurities and competing chloride oxidations pose challenges to the efficiency of water electrolysis. To overcome these difficulties, it is crucial to develop electrocatalysts with high activity, selectivity, and stability. Interface engineering has emerged as a promising strategy to surpass the limitations of single-component catalysts and achieve high-activity and stable electrocatalysts. Various approaches for creating interface effects have been reported, and the resulting electrocatalysts have demonstrated improved OER performance. This review highlighted the significant advancements achieved in interface engineering strategies for improving the efficiency of the OER in alkaline and seawater conditions. By classifying various interface structures and reviewing relevant studies, we demonstrated their positive contribution to OER performance. While additional research presented in Tables 1 and 2 showcases further efforts toward developing OER catalysts *via* interface engineering, a critical challenge remains: most catalysts currently lack the stability necessary for practical industrial applications.[87] Therefore, future research should focus on addressing these critical issues identified in this review to bridge the gap between promising laboratory results and real-world applications.

1) Understanding the intricate structure of interfacial regions and identifying active sites are key considerations in studying heterogeneous electrocatalysts. Catalysts produced through interface engineering exhibit complex compositions, which can make it challenging to discern the main active species involved in catalysis. Moreover, the formation of interfaces triggers multiple effects, such as lattice strain, defects, and modifications to the electronic structure, all of which can enhance catalytic performance.[24] However, these effects often occur simultaneously. Deconvoluting the interplay of various factors influencing OER performance remains a significant challenge. DFT calculations offer valuable insights into the atomic and electronic structures of catalysts, allowing researchers to predict the effects of specific configurations. Additionally, DFT calculations can estimate the Gibbs free energy of OER and CER intermediates on the catalyst surface, providing a deeper understanding of reaction mechanisms and facilitating the rapid development of high-performance catalysts in terms of activity, stability, and selectivity. However, constructing accurate simulations of complex, multi-component interfacial electrocatalysts remains challenging, leading to discrepancies between experimental and computational results. To bridge this gap, future research should focus on developing more sophisticated structural modeling techniques for DFT calculations.
2) OER catalysts often undergo dynamic phase transformations during operation, resulting in new materials with distinct morphologies, electronic structures, and phases. *In situ* characterization techniques, encompassing various microscopic and spectroscopic methods, provide real-time in-

Table 1. Summary of recently reported electrocatalysts through interface engineering for water oxidation in 1.0 M KOH.

Catalyst	Interface type	Overpotential (mV)	Stability (hours)	Ref.
NiFeV LDH	Doping	195@20 mA cm^{-2}	18@22 mA cm^{-2}	[40]
Gd–NiFe-LDH@CC	Doping	210@10 mA cm^{-2}	55@20 mA cm^{-2}	[41]
Se–FeOOH	Doping	348@500 mA cm^{-2}	100@100 mA cm^{-2}	[46]
O-NFO–S5	Doping	224@100 mA cm^{-2}	150@10 to 300 mA cm^{-2}	[47]
F–FeCoPv@IF	Doping	340@1 A cm^{-2}	–	[45]
CoP_3/Ni_2P	Compositional	337@100 mA cm^{-2}	40@50 mA cm^{-2}	[89]
(FeCoNi)OH–S/NF	Compositional	195@10 mA cm^{-2}	96@100 mA cm^{-2}	[90]
NiNS	Compositional	404@100 mA cm^{-2}	12@15 mA cm^{-2}	[91]
FNE300	Compositional	267@1 A cm^{-2}	50@100 mA cm^{-2}	[56]
$SnFeS_xO_y$/NF	Compositional	281@100 mA cm^{-2}	*ca.* 20@1.5 V	[92]
$FeSnCo_{0.2}S_xO_y$/NF	Compositional	186@10 mA cm^{-2}	70@9 mA cm^{-2}	[93]
Fe_2P–CoP/CeO_2-20	Morphology	248@10 mA cm^{-2}	30@25 mA cm^{-2}	[94]
$Co_{0.4}Ni_{1.6}P$–CeO_2/NF	Morphology	268@ 10 mA cm^{-2}	20@120 mA cm^{-2}	[65]
(Ni, Fe)S_2@MoS_2	Morphology	270@10 mA cm^{-2}	44@10 mA cm^{-2}	[95]
NiTe–NiFeN	Morphology	211@10 mA cm^{-2}	40@10 to 40 mA cm^{-2}	[68]
CoMoNiS–NF-31	Morphology	166@10 mA cm^{-2}	24@20 mA cm^{-2}	[96]
CoP@a-CoO_x	Amorphous-crystalline	232@10 mA cm^{-2}	24@10 mA cm^{-2}	[79]
c-CoFeP/a-CoFe LDH/NF	Amorphous-crystalline	293.4@500 mA cm^{-2}	85@100 mA cm^{-2}	[72]
c-$Ni_2P_4O_{12}$/a-$NiMoO_x$/NF	Amorphous-crystalline	250@20 mA cm^{-2}	42@10 mA cm^{-2}	[73]
CrO_x–Ni_3N	Amorphous-crystalline	308@50 mA cm^{-2}	36@40 mA cm^{-2}	[71]
Ni-ZIF/Ni–B@NF-4	Amorphous-crystalline	234@10 mA cm^{-2}	36@1.456 V	[75]

Table 2. Summary of recently reported electrocatalysts through interface engineering for seawater oxidation.

Catalyst	Interface type	Overpotential (mV)	Electrolyte	Stability (hours)	Ref.
$P_{4.8}$–NiFe ANs-400	Doping	305@500 mA cm^{-2}	Natural seawater	100@100 mA cm^{-2}	[48]
F–FeCoPv@IF	Doping	290@100 mA cm^{-2}	1.0 M KOH + seawater	100@100 mA cm^{-2}	[45]
Mn-doped Ni_2P/Fe_2P	Doping	270@100 mA cm^{-2}	1.0 M KOH + 0.5 M NaCl	200@500 mA cm^{-2}	[42]
S-(Ni,Fe)OOH	Doping	398@500 mA cm^{-2}	1.0 M KOH + seawater	100@100 mA cm^{-2}	[44]
NiFe-PBA-gel-cal	Compositional	329@100 mA cm^{-2}	1.0 M KOH + 0.5 M NaCl	60@50 mA cm^{-2}	[97]
Fe_2P/Ni_3N	Compositional	302@500 mA cm^{-2}	1.0 M KOH + seawater	40@500 mA cm^{-2}	[98]
FNE300	Compositional	291@1 A cm^{-2}	1.0 M KOH + seawater	50@100 mA cm^{-2}	[56]
$Fe_2P/Ni_{1.5}Co_{1.5}N/Ni_2P$	Compositional	307@500 mA cm^{-2}	1.0 M KOH + seawater	40@100 mA cm^{-2}	[55]
$Co_{0.4}Ni_{1.6}P$–CeO_2/NF	Morphology	394@ 200 mA cm^{-2}	1.0 M KOH + 0.5 M NaCl	20@1.6 V	[65]
(Ni, Fe)OOH@Ni_xP	Morphology	318@500 mA cm^{-2}	1.0 M KOH + seawater	100@500 mA cm^{-2}	[66]
NC–Ni_3N_{21}	Morphology	320@100 mA cm^{-2}	1.0 M KOH + seawater	500@1.77 V	[99]
$Co_{1.98}$–NiFe LDH	Amorphous-crystalline	335@100 mA cm^{-2}	1.0 M KOH + seawater	96@100 mA cm^{-2}	[78]
B–Co_2Fe LDH	Amorphous-crystalline	376@500 mA cm^{-2}	1.0 M KOH + seawater	100@ 500 mA cm^{-2}	[77]
NiFeO–CeO_2/NF	Amorphous-crystalline	322@1 A cm^{-2}	1.0 M KOH + 0.5 M NaCl	–	[86]
Ni_3FeOOH/Ni_3Fe-TPA/NF	Amorphous-crystalline	408@500 mA cm^{-2}	1.0 M KOH + seawater	24@10 mA cm^{-2}	[100]

sights into these evolving atomic and electronic structures, along with the behavior of OER adsorbates. This allows researchers to closely track changes in interfacial configurations throughout the OER process, which is crucial for deciphering the role of interfacial structures and guiding the rational design of OER catalysts. Ultimately, *in situ* characterization fosters a comprehensive understanding of how interfacial effects enhance OER catalysis.

3) Although interface engineering has demonstrated great potential in developing highly efficient OER electrocatalysts, most of the catalysts designed through this approach are currently limited to laboratory-scale applications due to their complex synthetic procedures. To enable their practical use in industrial applications, it is necessary to explore facile interface engineering approaches that allow for large-scale synthesis. The development of scalable and cost-effective methods is crucial for the widespread adoption of interface-engineered electrocatalysts.
4) Gaining a deeper understanding of natural seawater electrolysis is crucial for advancing the field. Most studies on seawater electrolysis have primarily focused on simulated electrolytes, which may not accurately represent the complex composition and conditions found in natural seawater. While some studies have explored the possibility of increasing OER selectivity by alkalizing natural seawater,[88] this approach introduces additional complexities and costs. Ultimately, achieving water electrolysis directly in natural seawater is desirable. However, the pH of natural seawater typically falls within the range of 8.0 to 8.3, which lacks the necessary OH^- ions for efficient OER. In this pH range, an additional process involving the adsorption and dissociation of water molecules becomes relevant, potentially reducing the overall efficiency of the OER. Consequently, it becomes challenging to avoid competing chloride oxidation reactions, and the presence of different ions in natural seawater can further impede the OER process. To address these challenges and develop effective OER catalysts, it is essential to study the OER pathway and the dynamics of ion diffusion in natural seawater. *In situ* characterization techniques and DFT calculations can provide valuable insights into the behavior of various ions and the OER process under realistic conditions. By combining experimental observations and theoretical modeling, researchers can gain a better understanding of the intricate mechanisms at play in natural seawater electrolysis.

Acknowledgements

The authors gratefully acknowledge the financial support from the Hong Kong Polytechnic University (Q-CDAG) and Shenzhen Key Basic Research Project, China (JCYJ20220818102210023). Daekyu Kim acknowledges the award of the Hong Kong PhD Fellowship.

Conflict of Interests

The authors declare that they have no known competing financial interests or personal relationships that could have appeared to influence the work reported in this paper.

Data Availability Statement

The data that support the findings of this study are available from the corresponding author upon reasonable request.

Keywords: interface engineering · oxygen evolution reaction · seawater splitting · electrocatalysis

[1] S. Chu, A. Majumdar, *Nature.* **2012**, *488*, 294–303.
[2] D. Shindell, C. J. Smith, *Nature.* **2019**, *573*, 408–411.
[3] F. Sun, J. Qin, Z. Wang, M. Yu, X. Wu, X. Sun, J. Qiu, *Nat. Commun.* **2021**, *12*, 4182.
[4] M. Aravindan, K. V. Madhan, V. S. Hariharan, T. Narahari, K. P. Arun, K. Madhesh, K. G. Praveen, R. Prabakaran, *Renew. Sustain. Energy Rev.* **2023**, *188*, 113791.
[5] J. Ran, M. Jaroniec, S.-Z. Qiao, *Adv. Mater.* **2018**, *30*, 1704649.
[6] F. Yu, H. Zhou, Y. Huang, J. Sun, F. Qin, J. Bao, W. A. Goddard, S. Chen, Z. Ren, *Nat. Commun.* **2018**, *9*, 2551.
[7] Z. Kang, H. Guo, J. Wu, X. Sun, Z. Zhang, Q. Liao, S. Zhang, H. Si, P. Wu, L. Wang, Y. Zhang *Adv. Funct. Mater.* **2019**, *29*, 1807031.
[8] B. You, Y. Sun Acc, *Chem. Res.* **2018**, *51*, 1571–1580.
[9] K. A. Stoerzinger, L. Qiao, M. D. Biegalski, Y. Shao-Horn, *J. Phys. Chem. Lett.* **2014**, *5*, 1636–1641.
[10] C. C. L. McCrory, S. Jung, J. C. Peters, T. F. Jaramillo, *J. Am. Chem. Soc.* **2013**, *135*, 16977–16987.
[11] S. Khatun, H. Hirani, P. Roy, *J. Mater. Chem. A* **2021**, *9*, 74–86.
[12] L. Yu, Q. Zhu, S. Song, B. McElhenny, D. Wang, C. Wu, Z. Qin, J. Bao, Y. Yu, S. Chen, Z. Ren, *Nat. Commun.* **2019**, *10*, 5106.
[13] S. Dresp, F. Dionigi, M. Klingenhof, P. Strasser, *ACS Energy Lett.* **2019**, *4*, 933–942.
[14] A. Bradshaw, K. Schleicher, *IEEE J. Oceanic Eng.* **1980**, *5*, 50–62.
[15] K. C. Kang, P. Linga, K.-n. Park, S.-J. Choi, J. D. Lee, *Desalination.* **2014**, *353*, 84–90.
[16] J. Yu, B.-Q. Li, C.-X. Zhao, Q. Zhang, *Energy Environ. Sci.* **2020**, *13*, 3253–3268.
[17] F. Dionigi, T. Reier, Z. Pawolek, M. Gliech, P. Strasser, *ChemSusChem.* **2016**, *9*, 962–972.
[18] J. N. Hausmann, R. Schlögl, P. W. Menezes, M. Driess, *Energy Environ. Sci.* **2021**, *14*, 3679–3685.
[19] M. Chen, N. Kitiphatpiboon, C. Feng, A. Abudula, Y. Ma, G. Guan, *eScience.* **2023**, *3*, 100111.
[20] Y. Zhang, Y. Lin, T. Duan, L. Song, *Mater. Today.* **2021**, *48*, 115–134.
[21] J. Choi, D. Kim, S. J. Hong, X. Zhang, H. Hong, H. Chun, B. Han, L. Y. S. Lee, Y. Piao, *Appl. Catal. B.* **2022**, *315*, 121504.
[22] J. Zhang, Q. Zhang, X. Feng, *Adv. Mater.* **2019**, *31*, 1808167.
[23] H. Xu, H. Shang, C. Wang, Y. Du Coord, *Chem. Rev.* **2020**, *418*, 213374.
[24] R. Zhao, Q. Li, X. Jiang, S. Huang, G. Fu, J.-M. Lee Mater, *Chem. Front.* **2021**, *5*, 1033–1059.
[25] W. Song, M. Li, C. Wang, X. Lu, *Carbon Energy.* **2021**, *3*, 101–128.
[26] L. Xiao, L. Qi, J. Sun, A. Husile, S. Zhang, Z. Wang, J. Guan, *Nano Energy.* **2024**, *120*, 109155.
[27] L. Xiao, Z. Wang, J. Guan, *Chem. Sci.* **2023**, *14*, 12850–12868.
[28] L. Xiao, Z. Wang, J. Guan, *Adv. Funct. Mater.* **2024**, *34*, 2310195.
[29] T. Tang, Z. Wang, J. Guan Coord, *Chem. Rev.* **2023**, *492*, 215288.
[30] J. Han, J. Guan, *Nano Res.* **2023**, *16*, 1913–1966.
[31] C. Xie, Z. Niu, D. Kim, M. Li, P. Yang, *Chem. Rev.* **2020**, *120*, 1184–1249.
[32] H. Li, C. Chen, D. Yan, Y. Wang, R. Chen, Y. Zou, S. Wang, *J. Mater. Chem. A.* **2019**, *7*, 23432–23450.
[33] Y. Yang, M. Luo, W. Zhang, Y. Sun, X. Chen, S. Guo, *Chem.* **2018**, *4*, 2054–2083.
[34] J. Liu, S. Duan, H. Shi, T. Wang, X. Yang, Y. Huang, G. Wu, Q. Li, *Angew. Chem. Int. Ed.* **2022**, *61*, e202210753.
[35] W. Tong, M. Forster, F. Dionigi, S. Dresp, R. Sadeghi Erami, P. Strasser, A. J. Cowan, P. Farràs, *Nat. Energy.* **2020**, *5*, 367–377.
[36] J. Guo, Y. Zheng, Z. Hu, C. Zheng, J. Mao, K. Du, M. Jaroniec, S.-Z. Qiao, T. Ling, *Nat. Energy.* **2023**, *8*, 264–272.
[37] A. Zhang, Y. Liang, H. Zhang, Z. Geng, J. Zeng, *Chem. Soc. Rev.* **2021**, *50*, 9817–9844.
[38] J. Tian, Y. Shen, P. Liu, H. Zhang, B. Xu, Y. Song, J. Liang, J. Guo, *J. Mater. Res. Technol.* **2022**, *127*, 1–18.
[39] Z. Gong, J. Liu, G. Ye, H. Fei, *Chem. Commun.* **2023**, *59*, 5661–5676.
[40] P. Li, X. Duan, Y. Kuang, Y. Li, G. Zhang, W. Liu, X. Sun, *Adv. Energy Mater.* **2018**, *8*, 1703341.
[41] M. Li, H. Li, X. Jiang, M. Jiang, X. Zhan, G. Fu, J.-M. Lee, Y. Tang, *J. Mater. Chem. A.* **2021**, *9*, 2999.
[42] Y. Luo, P. Wang, G. Zhang, S. Wu, Z. Chen, H. Ranganathan, S. Sun, Z. Shi, *Chem. Eng. J.* **2023**, *454*, 140061.
[43] M. Zhang, X. He, K. Dong, H. Zhang, Y. Yao, C. Yang, M. Yue, S. Sun, Y. Sun, D. Zheng, Y. Luo, Q. Liu, N. Li, B. Tang, J. Liu, X. Sun, *Chem. Commun.* **2023**, *59*, 9750–9753.
[44] L. Yu, L. Wu, B. McElhenny, S. Song, D. Luo, F. Zhang, Y. Yu, S. Chen, Z. Ren, *Energy Environ. Sci.* **2020**, *13*, 3439–3446.
[45] J. Zhu, J. Chi, T. Cui, L. Guo, S. Wu, B. Li, J. Lai, L. Wang, *Appl. Catal. B.* **2023**, *328*, 122487.
[46] S. Niu, W.-J. Jiang, Z. Wei, T. Tang, J. Ma, J.-S. Hu, L.-J. Wan, *J. Am. Chem. Soc.* **2019**, *141*, 7005–7013.
[47] X. Chen, Z. Qiu, H. Xing, S. Fei, J. Li, L. Ma, Y. Li, D. Liu, *Appl. Catal. B.* **2022**, *305*, 121030.
[48] L. Song, D. Zhang, H. Miao, Y. Shi, M. Wang, L. Zhao, T. Zhan, J. Lai, L. Wang, *Appl. Catal. B.* **2024**, *342*, 123376.
[49] J. Jiang, F. Sun, S. Zhou, W. Hu, H. Zhang, J. Dong, Z. Jiang, J. Zhao, J. Li, W. Yan, M. Wang, *Nat. Commun.* **2018**, *9*, 2885.
[50] J. Chang, G. Wang, Z. Yang, B. Li, Q. Wang, R. Kuliiev, N. Orlovskaya, M. Gu, Y. Du, G. Wang, Y. Yang, *Adv. Mater.* **2021**, *33*, 2101425.
[51] X. Luo, P. Ji, P. Wang, R. Cheng, D. Chen, C. Lin, J. Zhang, J. He, Z. Shi, N. Li, S. Xiao, S. Mu, *Adv. Energy Mater.* **2020**, *10*, 1903891.
[52] D. Yang, L. Cao, L. Feng, J. Huang, K. Kajiyoshi, Y. Feng, Q. Liu, W. Li, L. Feng, G. Hai, *Appl. Catal. B.* **2019**, *257*, 117911.
[53] J. Wang, M. Zhang, G. Yang, W. Song, W. Zhong, X. Wang, M. Wang, T. Sun, Y. Tang *Adv. Funct. Mater.* **2021**, *31*, 2101532.
[54] W. Ma, D. Li, L. Liao, H. Zhou, F. Zhang, X. Zhou, Y. Mo, F. Yu, *Small.* **2023**, *19*, 2207082.
[55] F. Zhang, Y. Liu, F. Yu, H. Pang, X. Zhou, D. Li, W. Ma, Q. Zhou, Y. Mo, H. Zhou, *ACS Nano.* **2023**, *17*, 1681–1692.
[56] L. Li, G. Zhang, B. Wang, D. Zhu, D. Liu, Y. Liu, S. Yang, *ACS Appl. Mater. Interfaces.* **2021**, *13*, 37152–37161.
[57] Y. Sun, W. Sun, G. Li, L. Wang, J. Huang, A. Meng, Z. Li, *J. Mater. Chem. A.* **2023**, *11*, 2262–2272.
[58] F. Pan, Y. Yang, *Energy Environ. Sci.* **2020**, *13*, 2275–2309.
[59] J. Choi, D. Kim, W. Zheng, B. Yan, Y. Li, L. Y. S. Lee, Y. Piao, *Appl. Catal. B.* **2021**, *286*, 119857.
[60] L. Liao, J. Sun, D. Li, F. Yu, Y. Zhu, Y. Yang, J. Wang, W. Zhou, D. Tang, S. Chen, H. Zhou, *Small.* **2020**, *16*, 1906629.
[61] C. Wang, L. Yu, F. Yang, L. Feng J Energy, *Chem.* **2023**, *87*, 144–152.
[62] L. Hu, X. Zeng, X. Wei, H. Wang, Y. Wu, W. Gu, L. Shi, C. Zhu, *Appl. Catal. B.* **2020**, *273*, 119014.
[63] P. Wang, Y. Luo, G. Zhang, Z. Chen, H. Ranganathan, S. Sun, Z. Shi, *Nano-Micro Lett.* **2022**, *14*, 120.
[64] X. Li, L. Xiao, L. Zhou, Q. Xu, J. Weng, J. Xu, B. Liu, *Angew. Chem. Int. Ed.* **2020**, *132*, 21292–21299.
[65] Y. Cong, X. Chen, Y. Mei, J. Ye, T.-T. Li, *Dalton Trans.* **2022**, *51*, 2923–2931.
[66] S. Zhang, Y. Wang, X. Wei, L. Chu, W. Tian, H. Wang, M. Huang, *Appl. Catal. B.* **2023**, *336*, 122926.
[67] Y. Bao, Z. Feng, K. Chen, D. Chen, D. Xu, Q. Wu, W. Li, J. Tu, *Int. J. Hydrogen Energy* **2024**, *51*, 1003–1010.
[68] R. Li, Y. Li, P. Yang, P. Ren, D. Wang, X. Lu, R. Xu, Y. Li, J. Xue, J. Zhang, M. An, J. Ma, B. Wang, H. Liu, S. Dou, *Appl. Catal. B.* **2022**, *318*, 121834.
[69] J. Kwon, H. Han, S. Jo, S. Choi, K. Y. Chung, G. Ali, K. Park, U. Paik, T. Song, *Adv. Energy Mater.* **2021**, *11*, 2100624.
[70] X. Zhang, Y. Li, Z. Wu, H. Sheng, Y. Hu, C. Li, H. Li, L. Cao, B. Dong, *Mater. Today Energy.* **2022**, *26*, 100987.
[71] M. Yang, M. Zhao, J. Yuan, J. Luo, J. Zhang, Z. Lu, D. Chen, X. Fu, L. Wang, C. Liu, *Small.* **2022**, *18*, 2106554.
[72] K. Zheng, J. Ren, X. Li, G. Li, L. Jiao, C. Xu, *Chem. Eng. J.* **2022**, *441*, 136031.
[73] J. Wang, J. Hu, S. Niu, S. Li, Y. Du, P. Xu, *Small.* **2022**, *18*, 2105972.
[74] G. Tian, S. Wei, Z. Guo, S. Wu, Z. Chen, F. Xu, Y. Cao, Z. Liu, J. Wang, L. Ding, J. Tu, H. Zeng, *J. Mater. Res. Technol.* **2021**, *77*, 108–116.
[75] H. Xu, B. Fei, G. Cai, Y. Ha, J. Liu, H. Jia, J. Zhang, M. Liu, R. Wu, *Adv. Energy Mater.* **2020**, *10*, 1902714.
[76] D.-C. Liu, L.-M. Cao, Z.-M. Luo, D.-C. Zhong, J.-B. Tan, T.-B. Lu, *J. Mater. Chem. A.* **2018**, *6*, 24920–24927.
[77] L. Wu, L. Yu, Q. Zhu, B. McElhenny, F. Zhang, C. Wu, X. Xing, J. Bao, S. Chen, Z. Ren, *Nano Energy.* **2021**, *83*, 105838.
[78] Y. Yang, S. Wei, Y. Li, D. Guo, H. Liu, L. Liu, *Appl. Catal. B.* **2022**, *314*, 121491.
[79] J. Yu, Y. Zhong, X. Wu, J. Sunarso, M. Ni, W. Zhou, Z. Shao, *Adv. Sci.* **2018**, *5*, 1800514.
[80] J. Hu, S. Li, Y. Li, J. Wang, Y. Du, Z. Li, X. Han, J. Sun, P. Xu, *J. Mater. Chem. A* **2020**, *8*, 23323–23329.

[81] Q. Li, Q. Chen, S. Lei, M. Zhai, G. Lv, M. Cheng, L. Xu, H. Xu, Y. Deng, J. Bao, *J. Colloid Interface Sci.* **2023**, *631*, 56–65.
[82] A. Dutta, S. Mutyala, A. K. Samantara, S. Bera, B. K. Jena, N. Pradhan, *ACS Energy Lett.* **2018**, *3*, 141–148.
[83] M. Kuang, J. Zhang, D. Liu, H. Tan, K. N. Dinh, L. Yang, H. Ren, W. Huang, W. Fang, J. Yao, X. Hao, J. Xu, C. Liu, L. Song, B. Liu, Q. Yan, *Adv. Energy Mater.* **2020**, *10*, 2002215.
[84] T. I. Singh, A. Maibam, D. C. Cha, S. Yoo, R. Babarao, S. U. Lee, S. Lee, *Adv. Sci.* **2022**, *9*, 2201311.
[85] D. Wu, B. Liu, R. Li, D. Chen, W. Zeng, H. Zhao, Y. Yao, R. Qin, J. Yu, L. Chen, J. Zhang, B. Li, S. Mu, *Small.* **2023**, *19*, 2300030.
[86] H. Zhang, Z. Bi, P. Sun, A. Chen, T. Wågberg, X. Hu, X. Liu, L. Jiang, G. Hu, *ACS Nano.* **2023**, *17*, 16008–16019.
[87] X. Lu, C. Zhao, *Nat. Commun.* **2015**, *6*, 6616.
[88] X. Xiao, L. Yang, W. Sun, Y. Chen, H. Yu, K. Li, B. Jia, L. Zhang, T. Ma, *Small.* **2022**, *18*, 2105830.
[89] J. Zhang, H. Zhou, Y. Liu, J. Zhang, Y. Cui, J. Li, J. Lian, G. Wang, Q. Jiang, *ACS Appl. Mater. Interfaces.* **2021**, *13*, 52598–52609.
[90] Y. Yang, M. Lin, Y. Wu, R. Chen, D. Guo, L. Liu J Colloid, *Interface Sci.* **2023**, *647*, 510–518.
[91] Y. Zhao, B. Jin, A. Vasileff, Y. Jiao, S.-Z. Qiao, *J. Mater. Chem. A.* **2019**, *7*, 8117–8121.
[92] T. Zhang, J. Han, T. Tang, J. Sun, J. Guan, *Int. J. Hydrogen Energy* **2023**, *48*, 4594–4602.
[93] S. Chen, T. Zhang, J. Han, H. Qi, S. Jiao, C. Hou, J. Guan, *Nano Res. Energy.* **2024**, *3*, e9120106.
[94] X. Ding, J. Yu, W. Huang, D. Chen, W. Lin, Z. Xie, *Chem. Eng. J.* **2023**, *451*, 138550.
[95] Y. Liu, S. Jiang, S. Li, L. Zhou, Z. Li, J. Li, M. Shao, *Appl. Catal. B.* **2019**, *247*, 107–114.
[96] Y. Yang, H. Yao, Z. Yu, S. M. Islam, H. He, M. Yuan, Y. Yue, K. Xu, W. Hao, G. Sun, H. Li, S. Ma, P. Zapol, M. G. Kanatzidis, *J. Am. Chem. Soc.* **2019**, *141*, 10417–10430.
[97] H. Zhang, S. Geng, M. Ouyang, H. Yadegari, F. Xie, D. J. Riley, *Adv. Sci.* **2022**, *9*, 2200146.
[98] W. Ma, D. Li, L. Liao, H. Zhou, F. Zhang, X. Zhou, Y. Mo, F. Yu, *Small.* **2023**, *19*, 2207082.
[99] A. Tewary, S. Mandal, Z. Alam, A. S. K. Sinha, U. Ojha, *ACS Sustainable Chem. Eng.* **2023**, *11*, 6556–6566.
[100] L. Xiao, X. Bai, J. Han, T. Tang, S. Chen, H. Qi, C. Hou, F. Bai, Z. Wang, J. Guan *Nano Res.* **2023**, https://doi.org/10.1007/s12274–023-6088-x.

Manuscript received: January 27, 2024
Revised manuscript received: March 25, 2024
Accepted manuscript online: March 25, 2024
Version of record online: April 19, 2024